DOI: 10.1002/((please add manuscript number))
Article type: Full paper

Solvent based Soft-Patterning of Graphene Lateral Heterostructures for Broadband High-Speed Metal-Semiconductor-Metal Photodetectors

Yang Xu[1,2†], Ayaz Ali[1†], Khurram Shehzad[1†], Nan Meng[1], Mingsheng Xu[3], Yuhan Zhang[4], Xinran Wang[4], Chuanhong Jin[5], Hongtao Wang[6], Yuzheng Guo[7], Zongyin Yang[2], Bin Yu[8], Yuan Liu[9], Qiyuan He[9], Xiangfeng Duan[9], Xiaomu Wang[10], Ping-Heng Tan[11], Weida Hu[12], Hai Lu[13] and Tawfique Hasan[2*]*

[1]State Key Laboratory of Silicon Materials & School of Information Science and Electronic Engineering, Zhejiang University, Hangzhou, Zhejiang 310027, China

[2]Department of Engineering, University of Cambridge, Cambridge CB3 0FA, UK

[3]Department of Polymer Science and Engineering, Zhejiang University, Hangzhou, Zhejiang 310027, China

[4]National Laboratory of Solid State Microstructures, School of Electronic Science and Engineering, and Collaborative Innovation Center of Advanced Microstructures, Nanjing University, Nanjing 210093, China

[5]School of Materials Science and Engineering, Zhejiang University, Hangzhou, Zhejiang 310027, China

[6]Institute of Applied Mechanics, Zhejiang University, Hangzhou, Zhejiang 310027, China

[7]Rowland Institute, Harvard University, 100 Edwin H Land Blvd, MA, 02142, USA

[8]College of Nanoscale Science and Engineering, State University of New York, Albany, New York 12203, USA

[9]Department of Chemistry and Biochemistry and California Nanosystems Institute, University of California, Los Angeles, California 90095, USA

[10]School of Engineering & Applied Science, Yale University, New Haven, CT 06511, USA

[11]State Key Laboratory of Superlattices and Micro structures, Institute of Semiconductors, Chinese Academy of Sciences, Beijing 100083, China

[12]National Laboratory for Infrared Physics, Shanghai Institute of Technical Physics, Chinese Academy of Sciences, Shanghai 200083, China

[13]Jiangsu Provincial Key Laboratory of Advanced Photonic and Electronic Materials, and School of Electronic Science and Engineering, Nanjing University, Nanjing 210093, China

† These authors contributed equally to this work.

*Corresponding Authors: Yang Xu, yangxu-isee@zju.edu.cn;Tawfique Hasan th270@cam.ac.uk

Abstract

Solvents are essential in synthesis, transfer, and device fabrication of two-dimensional materials (2d) and their functionalized forms. Controllable tuning of the structure and properties of these materials using common solvents could pave new and exciting pathways to fabricate high-performance devices. However, this is yet to be materialized as solvent effects on 2d materials are far from well-understood. Using fluorine functionalized CVD graphene (FG) as an example, and in contrast to traditional "hard-patterning" method of plasma etching, we demonstrate a solvent based "soft-patterning" strategy to enable its selective de-fluorination for the fabrication of graphene-FG lateral heterostructures with resolution down to 50 nm, in which the oxygen plasma etching process of patterning after graphene transfer is avoided and high quality surfaces are preserved through a physically continuous atomically thin sheet, which is critical for high performance photodetection, especially at high-speed domain. We further employ the fabricated lateral graphene heterostructures to demonstrate a high speed metal-semiconductor-metal photodetector (<10 ns response time), with a broadband response from deep UV (200nm) to near-infrared (1100 nm) range. Thanks to the high quality surface with much less defects obtained by "soft-patterning" strategy, we achieved a high deep-UV region photo-responsivity as well as the ultra-fast time response. Our strategy offers a unique and scalable method to realize continuous 2d lateral heterostructures, and underscores the significance of inspiring future designs for high speed optoelectronic devices.

Introduction

Solvents are ubiquitous in processes ranging from materials synthesis to device fabrication. In the context of graphene and other two-dimensional materials (2d), solvents play a key part in the synthesis[1],[2] (e.g., liquid-phase exfoliation), dispersion[3] and functionalization[4] for their final applications. Even for 2d materials synthesized by dry methods such as chemical vapor deposition (CVD), solvents are essential for transfer[5] and device fabrication.[6] While the importance of solvents is widely recognized in 2d materials processing, the exact role of solvents on materials and device performances is not well-understood. For example, although high quality defect-free graphene is generally thought to be unreactive towards common solvents, once in functionalized form (with hydrogen, oxygen, halogen, etc.), graphene can undergo a variety of reactions with solvents, including reduction[7], elimination[8], and substitution.[9] Such reactions can significantly alter the structure and properties of the functionalized graphene through change in nature and degree of functional group coverage.

Fluorine functionalized graphene (FG) is an important derivative of graphene due to its relatively higher thermal and chemical stability as compared with other functionalized forms.[10-12] A thorough review of FG is also recently published.[12] The binding of F radicals to graphene leads to surface activation and band gap opening[11-13], rendering the resultant FG useful for applications ranging from as a seed layer for dielectric deposition[14, 15] to as a growth precursor for synthesis of new 2d materials[16] and a building block for 2d heterostructures.[17] While FG, like some of the other functionalized graphene forms, holds great promises as a complementary material for next generation graphene-based electronics, it can readily de-fluorinate under humid conditions or when in contact with acetone[7, 18] Such a phenomenon, considering acetone an important solvent for FG transfer and patterning process, can seriously undermine the potential of FG for widespread application. This is because even

a marginal change in the degree of fluorine coverage on graphene can turn FG from an insulator to a semiconductor or even a conductor, drastically changing the function and performance of electronic devices. Here, we report a systematic investigation on the effect of different solvents (polar and non-polar, aqueous and organic) on the stability and de-fluorination of FG. Based on our results, we introduce a new solvent based "soft-patterning" strategy to fabricate sub 50 nm lateral graphene-FG heterostructures. Such strategy offers several advantages over e-beam based reductive patterning and plasma etch processing [19], such as, scalability, room temperature processing, high quality surface preserved, and avoids of creating more trapping states, which are critical in high-speed photodetection. We also demonstrate the successful integration of these lateral heterostructures for efficient optoelectronic devices by fabricating a state-of-the-art photodetector.

Results and Discussion

To explore the effect of solvents on FG, we start with the fluorination process. Figure 1a shows the changes in Raman signals and electrical resistivity of graphene fluorinated for different reaction times. Measurements carried out on graphene channels (L = 45 μm and W = 15 μm) show that as the fluorination time increases, the sheet resistance increases up to 10 GΩ/□, confirming increasing degree of fluorination. Changes in the Raman spectra with fluorination of graphene, such as emergence of disorder-induced D peak, changes in G, 2D peaks and the ratio of their intensities, i.e., I(D)/I(G) and I(2D)/I(G) (Fig. S1) indicate successful formation of FG (see supplementary section 1 for further details). The coverage of fluorine atoms on the graphene samples is uniform, as indicated by Raman mapping conducted on the graphene channels (inset of Fig. 1a). For the as-prepared FG on Cu foil, a maximum of ~24.5 % fluorinated carbon atoms are obtained, as measured by XPS (No Sulfur was detected in full XPS survey spectra shown in Fig. S2, confirming that dissociated S-

radicals from SF6 plasma didn't react with the graphene). Normalized spectrum weight (%) is obtained using deconvoluted C1s in to different components and area under the peak was used to calculate fluorinated carbon percentage using CASA XPS software. FG have three kinds of bonds (CF, CF_2, and CF_3), as shown in Fig. 1b. Mainly, CF_2 and CF_3 bonds are found in the CVD grown graphene due to structural defects, grain boundaries, edges or vacancy defects during the plasma fluorination process.[11, 20] (see supplementary section 2 for detailed XPS analysis).

To avoid the fluorination asscoiated damage to the Si substrate of devices, we fluorinate the graphene on Cu or Ni foils directly, before transferring the FG sample on to the Si based device. We find that after fluorination of CVD graphene on Ni/Cu substrates, its subsequent transfer by traditional PMMA method[21] and patterning alter its insulating properties. XPS measurement on the transferred FG (Fig. 1c) shows a strong decrease in intensity of F1s peak, indicating loss of F content [18] (from 24.5% in as-prepared FG on Cu foil to 4.4%). We attribute this to the loss of the insulating properties of transferred FG. The de-fluorination process is likely due to the reaction between F atoms on the graphene and the solvent (acetone) used during the transfer process. The de-fluorination of FG is further confirmed by Auger electron mapping (AES); see Fig. S4.

These results provide us impetus to study the effect of other commonly used solvents on de-fluorination of FG. For this purpose, as-prepared FGs on Cu foil are directly immersed in solvents, including deionized water (DIW), isopropanol (IPA), acetone, dichloromethane (DCM) and chloroform for a fixed immersion time of 30 min at room temperature. The samples are then characterized by XPS. The polarity of the solvents used is in the order of acetone > DIW > IPA > DCM > chloroform, with corresponding dipole moments of 2.88 > 1.85 > 1.66 > 1.60 > 1.04, respectively. After immersion in the solvent, XPS F1s peak intensity decreases and shifts marginally towards the lower binding energy (Fig. 1d). Solvent

dependent fluorine reduction is also confirmed from the decrease of percentage of all types of carbon-fluorine bonds (CF, CF_2 and CF_3) calculated from XPS spectra (Table S1). Considering the total fluorinated carbon atomic weight percentage (CF + CF_2 + CF_3) after immersion in different solvents, we further argue that FG is more reactive and tend to de-fluorinate in relatively more polar solvents (see Fig. S5 in supporting information).

Raman and electrical measurements also corroborate the observation on solvent polarity dependent de-fluorination of FG in solvents. For the same immersion time (1 hour), de-fluorination induced Raman changes including the recovery of intensity of 2D peak I(2D), decrease in intensity of D peak I(D) and reduction of full width at half maximum (FWHM) of all the specified peaks are more prominent in the relatively more polar solvents. For example, Fig. 1e clearly shows a much more prominent 2D peaks in acetone treated sample compared to that from the chloroform treated sample (more details on the effect of solvent polarity and immersion time on de-fluorination of FG can be found in S6). Similarly, the change in normalized sheet resistance for devices immersed in relatively polar solvent (acetone) for 60 min is more than 5 orders of magnitude, while it is less than ~2 orders of magnitude for devices immersed in relatively less (non) polar solvent (chloroform) for the same period (Fig. 1f., Fig. S7, and Fig. S10). To further study the electron transport mechanism, we tested the sheet resistance of FG devices under different temperature environment, ranging from 50 K to 300 K with steps of 25 K (Fig. S8). The as prepared FG device and FG immersed in less-polar solvents such as DCM shows insulating type behavior, with sheet resistance increasing with the decrease in temperature, an indication of hopping/tunneling between impurity states.[10] However, the FG device treated with highly polar solvent (acetone) recovers graphene like behavior (due to the removal of F atoms), where the sheet resistance increases with increasing temperature.[22] *Ab initio* molecular dynamics (MD) simulation in Fig. 2(a-c) also confirm that relatively more polar solvents such as DIW, acetone, and IPA can

completely or partially remove the F atoms, while less polar chloroform does not interact with it, which is in agreement with our experimental observations.

We argue that de-fluorination of FG in solvents does not take place via generally considered S_N1 and S_N2 nucleophile substitution reaction[9], as schematically shown in Fig. 2d. This is because substituting one functional group with another would not change the density of sp^3 or sp^2 carbon centers on graphene basal plane, and therefore, leading to no major change in conductivity. However, our results exhibit significant changes in electrical conductivity upon de-fluorination, implying that F is removed, not substituted. This is also confirmed by *ab initio* MD simulation, as discussed above. Removal of F would increase the density of sp^2 centers on graphene basal plane (Fig. S6), and would allow partial restoration of the electrically conducting conjugation networks. Moreover, XPS results of de-fluorinated graphene do not show the presence of any new element on graphene, further supporting our conclusion that F removal/elimination[8] is more probable mechanism of de-fluorination. However, it is challenging to confirm the fate of leaving F radicals/atoms as their concentration is too low to be detected by commonly used analytical methods. Our gas chromatography-mass spectrometry (GC-MS) characterization of the solvent (acetone) after reaction with as prepared FG sample did not detect any fluorine. Further, ascertaining the exact mechanism is further complicated due to the lack of a clear understanding of the structure of FG itself. [18] [7, 23]

Based on our observations from the solvents studied, we predict that in general all the solvents high on polarity index will tend to de-fluorinate FG, while solvents on low polarity index will mostly be unreactive and suitable for preserving structure and properties of FG. With rapid expansion of research and application of 2d materials, studies on the structure and properties of their functionalized forms will also expand.[24] We believe that insight into the

effect of solvents obtained here will also be helpful for synthesis, property characterization, and applications of functionalized forms of the other 2d materials.

The ability of polar solvents to effectively remove fluorine atoms opens a new pathway to fabricate graphene-FG lateral heterostructures by using polar solvents as a tool to selectively de-fluorinate FG. Here, we demonstrate photolithography patterned graphene-FG structures from pre-prepared FG film on SiO_2 substrate. We achieve this by selectively exposing areas of FG to DIW for 1 hour**.** The formation of graphene-FG lateral heterostructures is confirmed by AES mapping. The intensity distribution of F KLL Auger electron mapping clearly shows the formation of graphene-FG lateral heterostructures (Fig. 2e-2g) where the intensity of F KLL signal on FG area is much higher than that on the de-fluorinated area (and vice versa in C KLL Auger electron mapping). To further test the limit of our approach in terms of achieving various shape and size of patterned structures, we perform e-beam lithography and solvent assisted de-fluorination to fabricate graphene nanoribbons in graphene-FG lateral heterostructures, with widths ranging from few microns to sub 50 nm, as illustrated in SEM images in Fig. 2h. The light gray and dark colors in Fig. 2h represent the FG and graphene regions, respectively.[25]

The lateral graphene-FG heterostructures fabricated using our solvent assisted selective de-fluorination strategy are expected to provide several advantages. First, as we have demonstrated, the size and shape of the alternating regions of FG and graphene can be readily designed via lithography. Second, these heterostructures can be easily transferred[26] on to both flexible and non-flexible substrates for further applications (Fig. S11). Third and more importantly, the film with FG and graphene patterns is continuous with seamless boundaries between alternating graphene-FG structures, avoiding edges with dangling bonds and entanglements of micro-/nano-ribbons. Lastly, the boundary between FG and graphene is robust and chemically well-defined through the sp^3 C-F bonds. This is a significant advantage

over the graphene ribbons using conventional methods by oxygen plasma etching, which would include mixed sp^2 and sp^3 carbon bonds anchored with a variety of functional groups, compromising the device properties.

During the preparation of our manuscript, we came across a recently published interesting work on solvent effect on the de-fluorination of ultrasonically dispersed spongy graphene.[27] However, the scope of our work is fundamentally different as we focus on CVD graphene with systematic investigation and characterization, and more importantly, demonstrate an exciting new strategy to exploit the solvents as a tool for the fabrication of unprecedentedly high resolution lateral 2D heterostructures on continuous films for their use in high performance optoelectronic devices (as disscussed below).

As a demonstration of our lateral graphene-FG heterostructures for applications in high performance optoelectronic devices, we fabricate an interdigitated (IDT) Gr/Si/Gr (metal-semiconductor-metal) Schottky photodetector with equally-spaced 10 μm-wide graphene-FG fingers (device 'GR-FG') formed by selective-area de-fluorination using photolithography; Fig. 3a and S12. We first compare the GR-FG device with a reference metal-semiconductor-metal lateral graphene photodetector (device 'GR', namely, FG regions are etched away by oxygen plasma), having the same geometrical structure with 10 μm-wide graphene ribbon defined by oxygen plasma etching. To compare, for some devices, we also transferred a FG layer on the top of the GR-FG lateral heterostructures. Since FG is sensitive/reactive in ambient conditions[18], hence to improve the stability of FG devices, we coated on the top a 50 nm thick protective layer of aluminum oxide (Al_2O_3). The dark currents decrease from ~0.7 μA/cm^2 for the reference GR to ~0.4 μA/cm^2 forGR-FG devices (Fig. 3b). On the other hand, the photo-responsivity at −0.5 V bias increases from 0.13 A/W for the GR device to 0.22 A/W for the GR-FG device under an ultra-violet 375 nm laser illumination, showing an improvement of almost 160%. The obtained responsivity curves of GR and GR-FG are nearly

identical in shape (Fig. 3c.) However, the maximum responsivity at the wavelength of ~ 890 nm increases from 0.43 to 0.48 A/W for GR and GR-FG based devices. The responsivity change is more significant for shorter wavelengths (< 890 nm) than those for the longer wavelengths. Because the shorter wavelength is more sensitive to the surface states of lateral heterostructure, the better surface the higher responsivity. Our devices have much improved surface quality by using the solvent de-fluorination process, hence the responsivity at the shorter wavelengths is better than the longer wavelengths. Figure 3d shows that the noise-equivalent power (NEP) and corresponding specific detectivity of the GR-FG photodetector is improved by more than 60% on average (< 890 nm) compared to the reference GR photodetector. Importantly, our devices after Al_2O_3 coating showed a stable performance even after one year (Fig. S13). We have used a pulsed laser to investigate the response time of the GR-FG photodetector. Figure 4(a) shows the time-dependent behavior of the incident pulsed laser and the photocurrent of the photodetector. The zoom-in view of a laser pulse (Fig. 4b) shows that the pulse width is ~ 5 ns. The rise and fall time of the pulse are both < 2 ns, which qualifies our detectors as ultrafast, up to GHz frequency. Comparatively, GR device shows much slower response, even at the frequency as low as 10 kHz (Fig. S14). Our FG-GR lateral heterostructure photodetector qualifies all the parameters of a high performance photodetector with photocurrent NEP ≈ 7.3 pW/Hz$^{0.5}$, specific detectivity (D*) ≈ 6.7×10^9 Jones and more importantly, < 10 ns response time and > 90 dB linear-dynamic-region (LDR). We need point out that our FG-GR lateral photodetector has slightly large dark current density and lower specific detectivity compared to the preivous work[28-30] due to the relatively large leakage current commonly existed in metal-semiconductor-metal photodetectors.[31] Generally, different wavelength regimes are detected by separate photoactive semiconductors with appropriate bandgaps. It is noteworthy that our devices demonstrated consistent performance across the broad spectral range from deep ultra-violet (200 nm) to near-infrared (1100 nm).

Moreover, fast time response (< 10 ns) of our devices in this broad range also outperformed most of the previously reported graphene Schottky free-space (non-waveguide) UV photodetectors. A comparison with reported devices is presented in supplementary Table S2. It is important to mention that the device structures here are different from our previous work[28], which was a vertical graphene/Si heterostructure based photodetector, where electrons and holes are collected by graphene and bulk silicon, respectively. In contrast, in this work, the device structures are based on interdigitated patterned lateral metal-semiconductor-metal heterostructres, namely, graphene/Si/graphene structure, in which the lateral heterostructure is very sensitive to the surface states, especially at UV region and high speed domain, because both electrons and holes are collected by the surface graphene electrodes.

We attribute the origin of the performance improvement in responsivity, response time, and NEP to the continuous graphene-FG film fabricated by our soft-patterning strategy (room temperature de-fluorination by solvent) with seamless boundaries, which not only avoids the scattering and recombination effects arsing from dangling bonds (present in oxygen etched graphene ribbons) but also maximizes the effective detection area in IDT devices, desirable for high performance optoelectronic applications of 2d/3d van der Waals heterostructures. In comparison, the traditional subtractive lithography (hard-patterning) needs etching or/and ion bombardment[31], which significantly damages the van der Waals 2d heterostructures or degrades the surface quality of the underlying 3d substrate, leading to a large amount of surface trapping states and subsequent deterioration of the device performance in the high-speed domain, as shown in our GR Schottky photodetectors. We emphasize that in the deep UV region, due to the low penetration depth of the UV light (~ 10 nm), defects in graphene and Si interface could hinder the electron-hole pair seperation, which can seriously limit the responsivity of photodetetcors. However, for our devices, again thanks to the high quality

surface with much less defects obtained by soft-patterning strategy, we achieved a very high deep-UV region photo-responsivity as well as the ultra-fast time response. We find that transferring another layer of FG on top of the GR-FG lateral Schottky photodetector (denoted as 'FG on GR-FG' device) further improves the Schottky junction characteristics and overall performance of photodetector (responsivity ≈ 0.5 A/W, NEP ≈ 6.7 pW/Hz$^{0.5}$, D* ≈ 7.4×10^{9} Jones. We attribute this improvement to two factors. First, transferring FG upon the GR-FG device improves the conformal coverage of the lateral graphene-FG film on the silicon surface. This likely reduces the inhomogeneity of graphene/Si contact region. Second, charge transfer occurring between the top FG and the bottom graphene sections of graphene-FG layer due to the high electronegativity of fluorine atoms. We argue that this charge transfer enhances the *p*-type doping of the bottom graphene, improving the Schottky characteristics of the Graphene/Si junction. Such improvement of the junction quality with the integration of 2d graphene-FG heterostructures may offer a very effective strategy to engineer highly efficient optoelectronic devices.

Conclusions

We demonstrate that polar solvents, with their effective de-fluorination of FG, can be used as a tool for selective de-fluorination and therefore the "soft-patterning" of high resolution graphene-FG lateral heterostructures on continuous atomically thin sheets. In our "soft-patterning" strategy (selective de-fluorination by solvent), the oxygen plasma etching process is avoided and high quality surfaces (the CVD monolayer graphene and the naked silicon surface) and edges are preserved through a physically continuous atomically thin sheet, which is critical for high performance optoelectronic applications using 2d /3d van der Waals heterostructures, especially at high-speed domain. Such an outcome can be very important for next-generation 2d materials based devices, as exemplified by our state of the art

photodetector which has two outstanding benefits of ultras-fast time resposne and high responsivity in deep UV.

Material Section *(details are provided in supplementary materials and methods section)*

High quality monolayer CVD grown graphene is fluorinated by gentle remote plasma fluorination. Remote plasma fluorination of graphene, under different plasma power and reaction times, was monitored by Raman, XPS and electrical measurements. To check the effect of solvents, FG on Cu is immersed in various solvents for different durations. For photodetector fabrication, FG is transferred on prepared devices. Selective areas of FG on device are masked by spin coated PMMA and e-beam lithography. The exposed areas are dipped in solvents to selectively de-fluorinate the FG for the fabrication of lateral hetero-structures. XPS, SEM, AES and Raman Characterizations are performed for structural characterizations of FG and lateral hetero-structures. Electrical and opto-electrical measurements are performed on Agilent semiconductor device analyzer (B5100A), Keithley Source Meter 2450, and Thorlabs lasers with 375 nm and 532 nm wavelengths. The response time is measured by using trans-impedance amplifier (FEMTO DHPCA-100), periodic pulse laser (Edinburgh Instruments Ltd., EPL-Series, 375 nm and 470 nm), and an Agilent oscilloscope (DSO 9404A, 4GHz)

Supporting Information

Supporting Information is available from the Wiley Online Library or from the author.

Acknowledgements:

This work is supported by National Science Foundation of China (Grant Nos. 61274123, and 61474099), ZJ-NSF (LR12F04001) and micro-/nano-fabrication platform of ZJU University, and the Fundamental Research Funds for the Central Universities.

Received: ((will be filled in by the editorial staff))
Revised: ((will be filled in by the editorial staff))
Published online: ((will be filled in by the editorial staff))

References

[1] K.-G. Zhou, N.-N. Mao, H.-X. Wang, Y. Peng, H.-L. Zhang, *Angew. Chem. Int. Ed.* **2011**, *50*, 10839.
[2] T. Hasan, F. Torrisi, Z. Sun, D. Popa, V. Nicolosi, G. Privitera, F. Bonaccorso, A. C. Ferrari, *physica status solidi (b)* **2010**, *247*, 2953.
[3] J. N. Coleman, *Adv. Funct. Mater.* **2009**, *19*, 3680.
[4] C. Backes, N. C. Berner, X. Chen, P. Lafargue, P. LaPlace, M. Freeley, G. S. Duesberg, J. N. Coleman, A. R. McDonald, *Angew. Chem. Int. Ed.* **2015**, *54*, 2638.
[5] Y. Kim, H. Kim, T. Y. Kim, S. H. Rhyu, D. S. Choi, W. K. Park, C.-M. Yang, D. H. Yoon, W. S. Yang, *Carbon* **2015**, *81*, 458.
[6] Z. Cheng, Q. Zhou, C. Wang, Q. Li, C. Wang, Y. Fang, *Nano Lett.* **2011**, *11*, 767.
[7] J. H. Lee, G. K. W. Koon, D. W. Shin, V. E. Fedorov, J.-Y. Choi, J.-B. Yoo, B. Özyilmaz, *Adv. Funct. Mater.* **2013**, *23*, 3329.
[8] K. E. Whitener, R. Stine, J. T. Robinson, P. E. Sheehan, *J. Phys. Chem. C* **2015**, *119*, 10507.
[9] M. s. Dubecký, E. Otyepková, P. Lazar, F. e. Karlický, M. Petr, K. r. Čépe, P. Banáš, R. Zbořil, M. Otyepka, *J. Phys. Chem. Lett.* **2015**, *6*, 1430.
[10] R. R. Nair, W. Ren, R. Jalil, I. Riaz, V. G. Kravets, L. Britnell, P. Blake, F. Schedin, A. S. Mayorov, S. Yuan, *Small* **2010**, *6*, 2877.
[11] J. T. Robinson, J. S. Burgess, C. E. Junkermeier, S. C. Badescu, T. L. Reinecke, F. K. Perkins, M. K. Zalalutdniov, J. W. Baldwin, J. C. Culbertson, P. E. Sheehan, *Nano Lett.* **2010**, *10*, 3001.
[12] W. Feng, P. Long, Y. Feng, Y. Li, *Advanced Science* **2016**.
[13] O. Leenaerts, H. Peelaers, A. D. Hernández-Nieves, B. Partoens, F. M. Peeters, *Phys. Rev. B* **2010**, *82*, 195436.
[14] H. Guo, Y. Liu, Y. Xu, N. Meng, H. Wang, T. Hasan, X. Wang, J. Luo, B. Yu, *Nanotechnology* **2014**, *25*, 355202.
[15] X. Zheng, M. Zhang, X. Shi, G. Wang, L. Zheng, Y. Yu, A. Huang, P. K. Chu, H. Gao, W. Ren, Z. Di, X. Wang, *Adv. Funct. Mater.* **2015**, *25*, 1805.
[16] V. Urbanova, K. Hola, A. B. Bourlinos, K. Cepe, A. Ambrosi, A. H. Loo, M. Pumera, F. Karlicky, M. Otyepka, R. Zboril, *Adv Mater* **2015**, *27*, 2305.
[17] A. Geim, I. Grigorieva, *Nature* **2013**, *499*, 419.
[18] R. Stine, W.-K. Lee, K. E. Whitener Jr, J. T. Robinson, P. E. Sheehan, *Nano Lett.* **2013**, *13*, 4311.
[19] F. Withers, T. H. Bointon, M. Dubois, S. Russo, M. F. Craciun, *Nano Lett.* **2011**, *11*, 3912.
[20] B. Wang, J. Wang, J. Zhu, *ACS Nano* **2014**, *8*, 1862.
[21] J. W. Suk, A. Kitt, C. W. Magnuson, Y. Hao, S. Ahmed, J. An, A. K. Swan, B. B. Goldberg, R. S. Ruoff, *ACS Nano* **2011**, *5*, 6916.
[22] K. Tahara, T. Iwasaki, S. Furuyama, A. Matsutani, M. Hatano, *Appl. Phys. Lett.* **2013**, *103*, 143106.
[23] D. O'Hagan, *Chem. Soc. Rev.* **2008**, *37*, 308.
[24] S. Lei, X. Wang, B. Li, J. Kang, Y. He, A. George, L. Ge, Y. Gong, P. Dong, Z. Jin, *Nat. Nanotechnol.* **2016**, *11*, 465.

[25] Y. Wang, Y. Shen, X. Zhang, Y. Zhang, J. Hu, *Appl. Phys. Lett.* **2014**, *105*, 233107.
[26] H. Li, J. Wu, X. Huang, Z. Yin, J. Liu, H. Zhang, *ACS Nano* **2014**, *8*, 6563.
[27] X. Wang, W. Wang, Y. Liu, M. Ren, H. Xiao, X. Liu, *Phys. Chem. Chem. Phys.* **2016**, *18*, 3285.
[28] T. Yu, F. Wang, Y. Xu, L. Ma, X. Pi, D. Yang, *Adv. Mater.* **2016**, *28*, 4912.
[29] L.-B. Luo, L.-H. Zeng, C. Xie, Y.-Q. Yu, F.-X. Liang, C.-Y. Wu, L. Wang, J.-G. Hu, *Scientific Reports* **2014**, *4*, 3914.
[30] X. Li, M. Zhu, M. Du, Z. Lv, L. Zhang, Y. Li, Y. Yang, T. Yang, X. Li, K. Wang, H. Zhu, Y. Fang, *Small* **2016**, *12*, 595.
[31] Y. An, A. Behnam, E. Pop, A. Ural, *Appl. Phys. Lett.* **2013**, *102*, 013110.

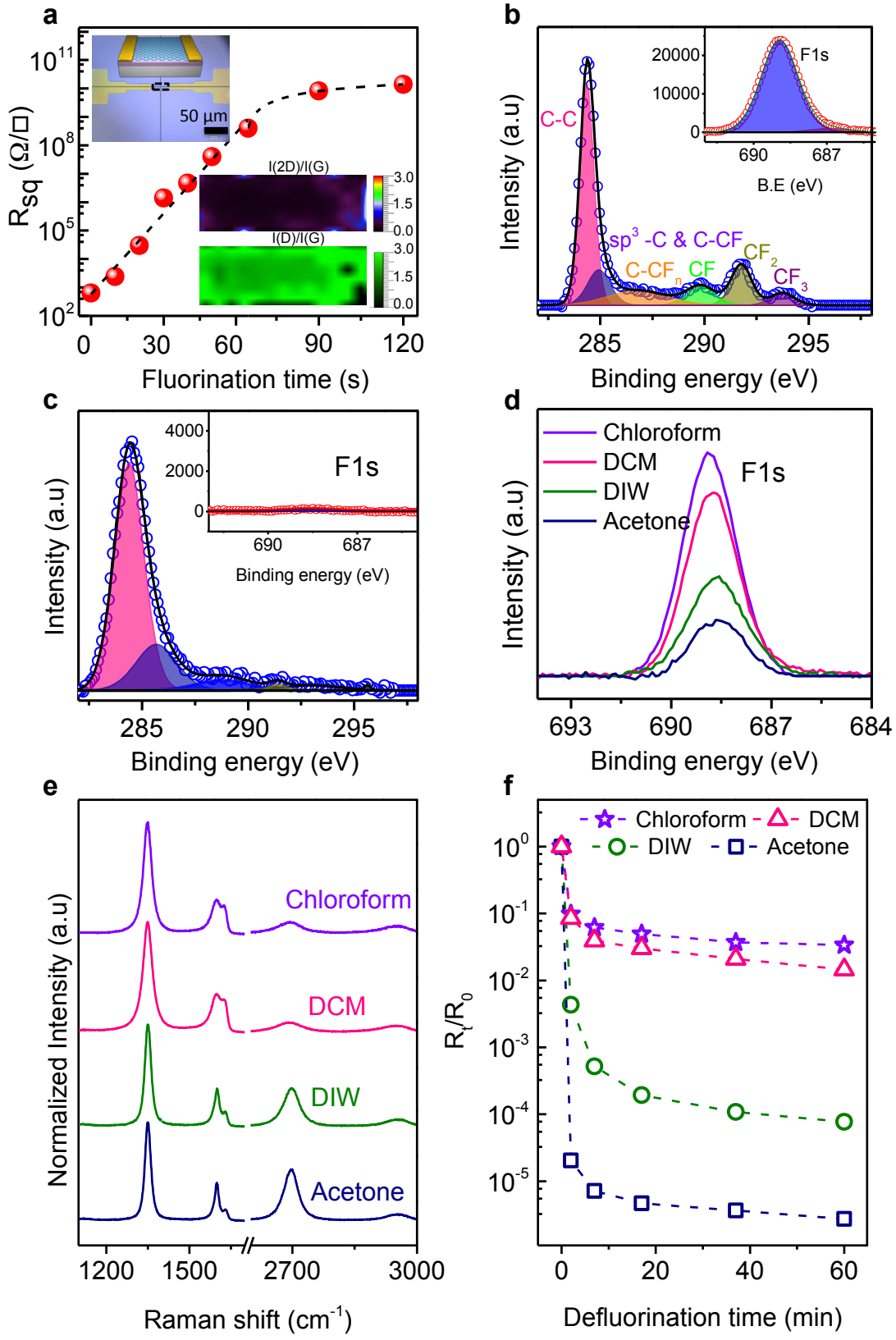
a
R_{sq} (Ω/□)
10^{11}
10^{8}
10^{5}
10^{2}
50 μm
I(2D)/I(G)
3.0
1.5
0.0
I(D)/I(G)
3.0
1.5
0.0
0
30
60
90
120
Fluorination time (s)
b
Intensity (a.u)
C-C
sp^3 -C & C-CF
$C-CF_n$
CF
CF_2
CF_3
20000
10000
0
F1s
690
687
B.E (eV)
285
290
295
Binding energy (eV)
c
Intensity (a.u)
4000
2000
0
F1s
690
687
Binding energy (eV)
285
290
295
Binding energy (eV)
d
Chloroform
DCM
DIW
Acetone
F1s
Intensity (a.u)
693
690
687
684
Binding energy (eV)
e
Normalized Intensity (a.u)
Chloroform
DCM
DIW
Acetone
1200
1500
2700
3000
Raman shift (cm^{-1})
f
Chloroform
DCM
DIW
Acetone
R_t/R_0
10^{0}
10^{-1}
10^{-2}
10^{-3}
10^{-4}
10^{-5}
0
20
40
60
Defluorination time (min)

Figure 1. (a) Graphene sheet resistance as the function of fluorination time, inset is an optical image and Raman mapping of a FG device channel. **(b)** XPS spectra of as synthesized FG on Cu foil (25W, 2 min), and **(c)** after transfer on Si substrate. **(d)** High resolution XPS F1s spectra of FG treated in different solvents for fixed immersion time of 30 minutes. **(e)** Raman spectra of FG sample treated with solvents for 1 hour. **(f)** Normalized sheet resistance of FG devices after treatment in different solvents for various times.

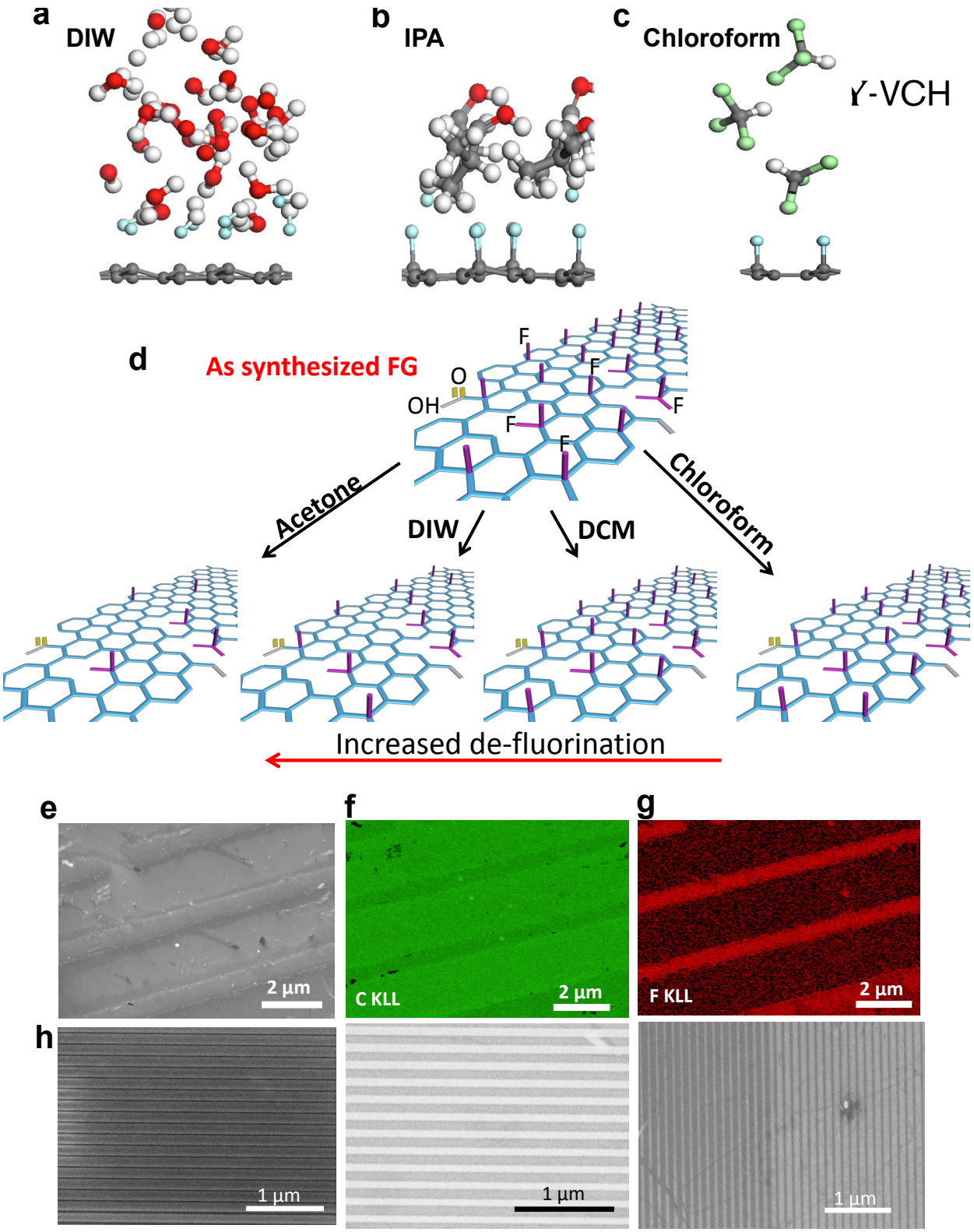

Figure 2. (a-c) Typical *ab initio* MD snapshots of the de-fluorination process after 0.2 ns simulation run. Carbon, hydrogen, oxygen, fluorine, and chlorine atoms are represented as grey, white, red, cyan, and green balls, respectively. The simulation shows that: **(a)** DIW can completely remove the F atoms from the FG. **(b)** IPA can remove a fraction of F atoms. **(c)** Chloroform is inert and does not interact with the FG. **(d)** Schematic of as-synthesized FG

and degree of de-fluorination in the solvents studied here. **(e)** SEM image of graphene and FG lateral heterostructure. **(f, g)** AES mapping of C KLL and F KLL signals, respectively. **(h)** SEM images graphene nanoribbons with varying ribbon width obtained using selective area de-fluorination of FG in DIW for 1 hour.

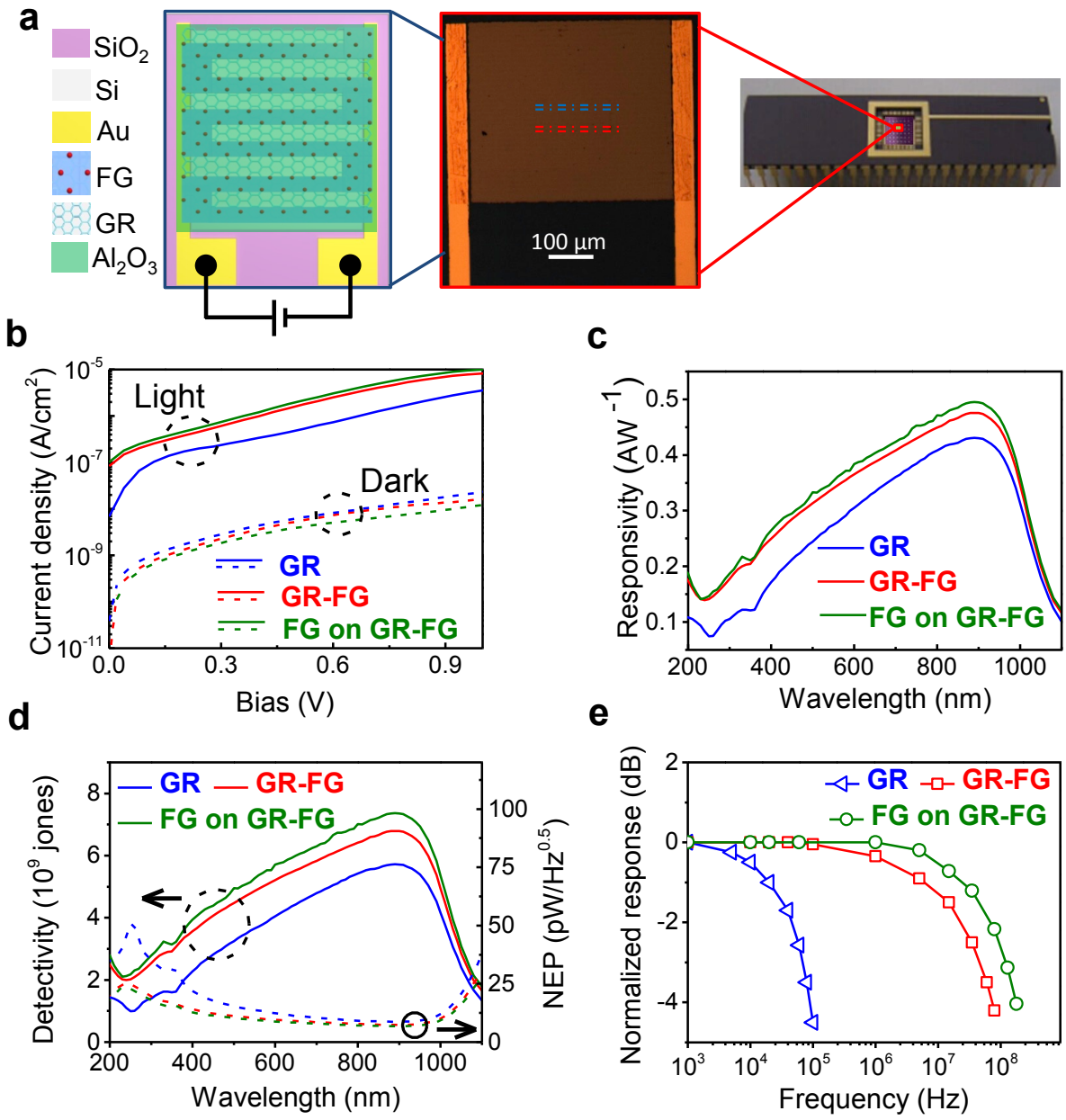

Figure 3. (a) Schematics, optical image, and photograph of photodetector arrays of interdigitated (IDT) lateral patterned photodetector fabricated using selective-area de-fluorination of post-transferred monolayer FG on Si. **(b)** The dark currents of the three

photodetectors (dotted lines) and their photocurrents (solid lines) are compared. **(c)** Responsivity of the three lateral photodetectors, namely, GR, GR-FG and FG on GR-FG. **(d)** Noise-equivalent-power (NEP) and specific detectivity of the GR, GR-FG and FG on GR-FG photodetectors. **(e)** Frequency response of the photodetectors based on etched Gr ribbons (blue line), GR-FG lateral heterostructures (red lines) and FG transferred upon GR-FG device (dark green).

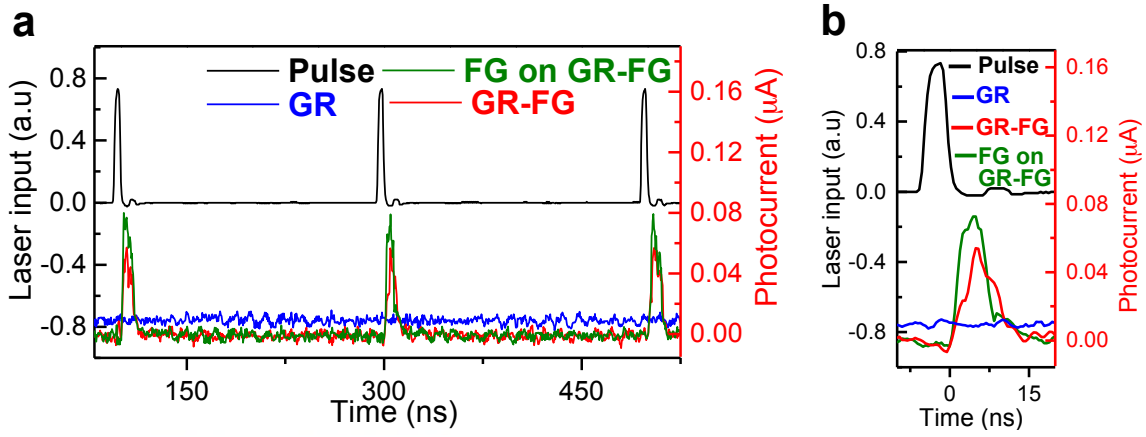

Figure 4. **(a)** Time-dependent behavior of the incident laser light and the photocurrent of the three lateral photodetectors, namely, GR, GR-FG and FG on GR-FG. **(b)** Zoom-in view of a laser pulse and the time-dependent photocurrent of the three lateral photodetectors, namely, GR, GR-FG and FG on GR-FG, responding to single laser pulse. The response speed is improved from GR to GR-FG by ~3 orders, supporting the advantages of "soft-patterning" strategy based on selective de-fluorination.